Bistability and torus break-up in a semiconductor laser with phase-conjugate feedback

Kirk Green and Bernd Krauskopf

Department of Engineering Mathematics, University of Bristol, Bristol BS8 1TR, UK

Koen Engelborghs

Department of Computer Science, K. U. Leuven, Celestijnenenlaan 200A, 3001 Heverlee, Belgium

Abstract

We present a detailed study of a route to chaos via quasiperiodicity on a torus in a semiconductor laser with phase-conjugate feedback. Highlighting the use of new tools that go far beyond mere simulation, we compute bifurcation diagrams and unstable manifolds of saddle periodic orbits. In this way, we show how a torus breaks up with a final sudden onset of chaos in a crisis bifurcation. We also identify regions of bistability between periodic solutions and other attractors in the system.

Key words: Lasers with delay, crisis bifurcation, continuation, unstable manifolds
PACS: 42.65.Hw, 42.65.Sf, 02.30.Ks

1 Introduction

Semiconductor lasers with delay [1,2] are technologically important examples of physical systems described by delay differential equations (DDEs) [3–6]. Such lasers are used in many physical applications, including CD players, laser printers and optical communication networks. Delay generally arises by optical reflection on an external reflector such as a CD or an optical fibre,

Email addresses: kirk.green@bristol.ac.uk (Kirk Green), b.krauskopf@bristol.ac.uk (Bernd Krauskopf), koen.engelborghs@cs.kuleuven.ac.be (Koen Engelborghs).

so that the laser 'sees' its past output after a fixed time delay. Examples of lasers with delayed feedback include the case of *conventional optical feedback* (COF) from an external mirror [7,8], mutually coupled lasers with delay [9], lasers with opto-electronic feedback [10] and lasers with *phase conjugate feedback* (PCF) from an external *phase conjugating mirror* (PCM) [11–16]. In many applications chaotic output is unwanted, and expensive optical isolators need to be used. However, recently there has been considerable interest in the controlled production of chaotic optical output for use in chaotic communication schemes [17,18]. In general, an understanding of the dynamics of a semiconductor laser with feedback can lead to new uses and better control of lasers. Considering the vast amount of lasers used in applications, this is of a considerable economical interest.

Our object of study is a semiconductor laser with PCF, schematically shown in Figure 1. This form of feedback is interesting as it produces a reflected wave that is wave-front inverted, with the angle of incidence of the wave being equal to the angle of reflection. Furthermore, any distortions in the external cavity are undone over a round-trip, thus the amplified beam is less spread and the energy more focused than with COF [11]. Also, compared to COF, where there is extreme sensitivity to the positioning of the mirror, PCF lasers are 'self-aligning'; this is an advantage when stable output is desired. Physical applications of PCF include mode locking [12] and phase locking, where PCF has been shown to reduce the laser noise considerably [13–15]. The PCF laser has been shown to exhibit a wealth of dynamics, including stable periodic operation, quasiperiodic motion and chaos [15,16]. Transitions to chaos were recently studied by simulation, with a combination of bifurcation diagrams and phase-plots [16]. However, a question remains, 'What are the global dynamics underlying these transitions?'. To answer this question, we need to use numerical tools that go beyond simulation.

In this paper, we use new and advanced numerical tools for DDEs to investigate the PCF laser. We concentrate on a transition involving the break-up of a torus and show in Section 6 that a *crisis bifurcation* is responsible for a sudden transition to chaos: a regular small attractor (a hose-like torus) increases dramatically in size and becomes a large chaotic attractor. Our study is made possible by, firstly, the package DDE-BIFTOOL [19–21], which allows one to perform continuation and bifurcation analysis of DDEs, much like AUTO [22] does for ordinary differential equations (ODEs). Our second main tool is to compute one-dimensional (1D) unstable manifolds of saddle periodic orbits in systems of DDEs [23]. These unstable manifolds are important for understanding the global dynamics of dynamical systems. These tools are described in more detail in Section 3.

A further goal of this paper is to showcase these advanced numerical techniques. Our approach not only applies to the PCF laser, but can be used in

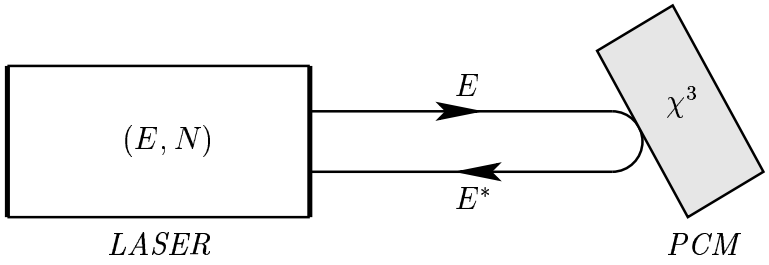

Fig. 1. A semiconductor laser with phase-conjugate feedback.

others areas of science and engineering in which DDEs are being increasingly used to model physical phenomena. These include areas as diverse as biology [24], neural networks [25] and control theory [26]. Note that advanced tools have not been widely used, first examples of the use of DDE-BIFTOOL include the studies of a COF laser in Refs. [27–30], of a vertical-cavity surface emitting laser in Ref. [31], and of a PCF laser here and in Refs. [32,33]. Furthermore, we extended the capabilities of DDE-BIFTOOL to deal with the specific properties of the equations under consideration. Manifold computations for periodic orbits of DDEs are presented here for the first time.

The paper is organised as follows. In Section 2 we introduce rate equations for a semiconductor laser with PCF; we also give a short introduction to the mathematics of DDEs. In Section 3 we introduce the advanced numerical tools we use. In Section 4 we show bifurcation diagrams obtained by simulation and by continuation to provide an outline of the dynamics involved in a route to chaos in the system. This leads to the discovery of regions of bistability which we detail in Section 5. In Section 6 we compute unstable manifolds of locked periodic orbits and show that the mechanism behind the transition to chaos is due to the break-up of a torus culminating in a crisis bifurcation. Finally, we draw conclusions and discuss future work in Section 7.

2 Semiconductor Laser with Phase-Conjugate Feedback

A single-mode semiconductor laser with PCF can be described by the three-dimensional delay differential system

$$\begin{aligned}\frac{dE}{dt} &= \frac{1}{2}\left[-i\alpha G_N(N(t)-N_{\mathrm{sol}}) + \left(G(t)-\frac{1}{\tau_p}\right)\right]E(t) \\ &\qquad +\kappa E^*(t-\tau)\exp[2i\delta(t-\tau/2)+i\phi_{\mathrm{PCM}}] \\ \frac{dN}{dt} &= \frac{I}{q} - \frac{N(t)}{\tau_e} - G(t)\,|E(t)|^2\end{aligned} \tag{1}$$

for the evolution of the slowly varying complex electric field $E(t)$ and the population inversion $N(t)$ [15,16]. In system (1), nonlinear gain is included as $G(t) = G_N(N(t) - N_0)(1 - \epsilon P(t))$, where $\epsilon = 3.57 \times 10^{-8}$ is the nonlinear gain coefficient and $P(t) = |E(t)|^2$ is the intensity. Parameter values are set to realistic values corresponding to a Ga-Al-As semiconductor laser [15,16], namely, the line-width enhancement factor $\alpha = 3$, the optical gain $G_N = 1190\,\mathrm{s}^{-1}$, the photon lifetime $\tau_p = 1.4\,\mathrm{ps}$, the injection current $I = 65.1\mathrm{mA}$, the magnitude of the electron charge $q = 1.6 \times 10^{-19}\mathrm{C}$, the electron lifetime $\tau_e = 2\mathrm{ns}$, and the transparency electron number $N_0 = 1.64 \times 10^8$. Further, $N_{\mathrm{sol}} = N_0 + 1\,/\,(G_N\tau_p)$. The constant phase shift ϕ_{PCM} at the PCM and the detuning parameter δ were both set to zero, as is common in the field [15,16]. Therefore, the feedback term in system (1) reduces to $\kappa E^*(t-\tau)$ and involves the complex conjugated electric field E^*, the feedback rate κ and the external cavity round-trip time τ. We fix τ at the realistic value $\tau = 2/3\,\mathrm{ns}$ and consider the dimensionless bifurcation parameter $\kappa\tau$.

System (1) has $\mathbb{Z}_2$-symmetry under the transformation $E \to -E$, where the symmetry group is $\mathbb{Z}_2 = \{1, -1\}$. This corresponds to a rotation over π of the complex E-plane, so that any attractor (or other invariant set) is either symmetric, or has a symmetric counterpart. This symmetry allows the possibility of symmetry-breaking and symmetry-restoring bifurcations [16,34], and also implies restrictions on the types of bifurcations of periodic orbits. For example, symmetric orbits cannot undergo period-doubling bifurcations [35]. The numerical consequences of this symmetry are described in Section 3.

2.1 Delay Differential Equations

System (1) is a system of DDEs. We now introduce some notation and recall some concepts of DDEs, where we follow [3–6,23]. The phase space of a DDE is infinite-dimensional. A *state* q of the system is a continuous function on the time interval $[-\tau, 0]$ with values in (E, N)-space. In other words

$$q \equiv \{\, (E(t), N(t)) \mid t \in [-\tau, 0] \,\}.$$

We call $q(0)$ the *head-point* of q and $\{q(t) \mid t \in [-\tau, 0)\}$ its *history*. A state q, that is, knowledge of (E, N) over the entire interval $[-\tau, 0]$, uniquely determines the dynamics of system (1) for $t \in [-\tau, \infty)$. In other words, q is an initial condition. While (E, N)-space is not the phase space of system (1), it is nevertheless helpful to show trajectories projected onto (E, N)-space, which is also called the physical space.

An *equilibrium* of system (1) is a solution $(E(t), N(t)) = (E_0, N_0)$ for all $t \in [-\tau, \infty)$ and fixed $(E_0, N_0) \in \mathbb{R}^3$, so that the right hand side of system (1) is zero. The stability of an equilibrium is given by the eigenvalues

of the linearization of system (1) around (E_0, N_0). There are infinitely many eigenvalues, but only finitely many with positive real part. Consequently, there are only finitely many unstable eigenfunctions.

The main object of study in this paper are *periodic solutions* of system (1). A periodic solution is a solution along which any state q is mapped to itself after integration of system (1) over time T, called the period. The stability of a periodic solution is given by its Floquet multipliers, which are the eigenvalues of the linearization of system (1) along the periodic orbit. Again, there are infinitely many eigenvalues, but only finitely many outside the unit circle, i.e. again there are only finitely many unstable eigenfunctions.

Near a periodic orbit, one can define the *Poincaré map* P which maps a state q with head-point in a suitable section Σ to $P(q)$, which is again a state with head-point in Σ. In other words, for $q(0) \in \Sigma$ then $P(q(0)) \in \Sigma$, where $P(q)$ is another state. Therefore, P is an infinite-dimensional map on the space of states with head-points in Σ.

The *unstable manifold* $W^u(q)$, of the saddle periodic state q, is the set of all states p that can be iterated backwards under P and reach q in the limit. That is, $P^m(p) \to q$ as $m \to -\infty$. We remark that it is generally not possible to integrate a DDE backwards in time. However, for $W^u(q)$ it is possible, which is part of its definition; see Refs. [4,5]. In the case of one Floquet multiplier outside the unit circle, the unstable eigenfunction of q is unique and, in projection onto (E, N)-space, the 1D linear eigenspace $E^u(q)$ forms a one-parameter family of directions along the state q. The *trace* $W_u(q) \cap \Sigma$ is a smooth 1D curve (except possibly at isolated points due to projection) that reveals as much about the dynamics as a 1D unstable manifold of a saddle point of a diffeomorphism in $\mathbb{R}^2$; see Ref. [23] for details.

3 Advanced Numerical Tools for DDEs

The basic operation one needs to perform is numerical integration of system (1). In order to integrate this DDE, we discretize the state q on the time interval $[t - \tau, t]$ into M subintervals, leading to an integration time-step of τ/M. In our simulations we use an Adams-Bashforth fourth-order multistep method [23], which requires knowing values up to and including $q(-\tau - 3\frac{t}{M})$ for a single integration step; we set $M = 2500$. To start an integration, we can use either a random initial condition, or initial conditions obtained from a previous simulation or via continuation. Furthermore, in our study we make use of recent developments in the theory and numerics of DDEs.

3.1 Continuation

We use the continuation package DDE-BIFTOOL [19–21], consisting of Matlab routines, for the bifurcation analysis of steady states and periodic solutions. This not only allows us to find and follow stable solutions (those one also finds by simulation), but also unstable ones. Furthermore, DDE-BIFTOOL detects local bifurcations. For equilibria, these bifurcations are: a saddle-node bifurcation when a real eigenvalue changes sign and a Hopf bifurcation when a complex pair of eigenvalues cross the imaginary axis. For periodic solutions, these bifurcations are: a saddle-node bifurcation of limit cycles when a real Floquet multiplier crosses the unit circle at $+1$, a period-doubling bifurcation when a real Floquet multiplier crosses the unit circle at -1 and a torus (Neimark-Sacker) bifurcation when a pair of complex Floquet multipliers cross the unit circle. It is possible to compute bifurcating branches of periodic orbits from detected bifurcation points.

Because of the $\mathbb{Z}_2$-symmetry, it is possible that a Floquet multiplier crossing $+1$ corresponds to a symmetry-breaking bifurcation. In order to deal with symmetry-breaking bifurcations, we extended DDE-BIFTOOL to allow branch switching at symmetry-breaking bifurcations as well. There is now a routine to compute the linearised direction corresponding to this multiplier. Specifically, it is found by computing the eigenvalues of the discretized monodromy operator. The eigenfunction which is thus found is defined on the delay interval $[-\tau, 0]$ and is further integrated under the linearized equations to obtain a profile on the complete period interval $[0, \mathsf{T}]$. The eigenfunction can then be used as a perturbation in the direction of the emanating branch to provide a guess of an initial solution on the branch. It is also used in a special steplength condition to prevent convergence of the computation back to the original branch. During these computations, the continuation parameter is also corrected. As such, the branch switching automatically detects the direction of the emanating branch (to higher or lower values of the continuation parameter). After a first point is found, the branch can then be continued further.

For computing periodic solutions and their stability, DDE-BIFTOOL uses orthogonal collocation based on a piecewise polynomial representation on adapted meshes, a technique also used in the well-known continuation package AUTO [22]. This technique computes a periodic solution using a discrete periodic representation satisfying the differential equation at a given, finite set of points. In our tests we used polynomials of degrees 3 and 4 on meshes with 150 subintervals (200 for the period-doubled branches). Note that similar computational accuracy can only be expected on a period-doubled branch (compared to the original branch) when the mesh size is doubled. The accuracy of the obtained solutions was checked by comparing results on finer

meshes. The accuracy of the trivial Floquet multiplier, equal to +1 and corresponding to a phase shift along the periodic orbit, was always checked to be below 0.001 over the computed branches.

3.2 1D Unstable Manifolds

Our second main tool is a new technique for computing 1D unstable manifolds of saddle periodic orbits. Specifically we compute the 1D unstable manifold $W^u(q)$ of an associated fixed point q of a suitable Poincaré map defined on a fixed section Σ. This allows us, for the first time in DDEs, to compute certain invariant objects, for example, an underlying torus on which the dynamics is attracted to a stable periodic orbit. Unstable manifolds are of great importance in understanding the global dynamics of a system. However, they cannot be found analytically and therefore, need to be computed by numerical methods. Our method generalizes a well established algorithm for computing 1D unstable manifolds in ODEs [36]. It grows the unstable manifold such that the headpoints in Σ are a distance Δ_k apart. The distance Δ_k is constantly adapted according to the curvature of $W^u(q) \cap \Sigma$, thus providing a best possible numerical approximation given prespecified accuracy parameters. Since each intersection point of the unstable manifold in Σ has an associated history of length τ, the projection of the unstable manifold into the physical (E, N)-space forms a very complicated object. However, the trace $(W^u(q) \cap \Sigma)$ of the 1D unstable manifold in Σ is a smooth 1D curve (with the exception of some points, where smoothness may be lost due to the projection).

For a detailed explanation of this method and the associated accuracy parameters see Ref. [23]. For the computations in this paper, we set a lower bound on Δ_k of $\Delta_{\min} = 1.0$, where the range of the E-plane is of order 10^2. In the notation of [23], other accuracy parameters controlling the angle α_k between the lines through three consecutive points on the manifold and the local interpolation error $\Delta\alpha_k$ were set to $\alpha_{\min} = 0.2$, $\alpha_{\max} = 0.3$, and $(\Delta\alpha)_{\min} = 1.0 \times 10^{-2}$, $(\Delta\alpha)_{\max} = 1.0 \times 10^{-1}$. The parameter ϵ which reduces the number of bisection steps during computation was set to $\epsilon = 0.2$ and the initial distance δ along $W^u(q)$ was chosen in $[0.001, 0.04]$. If Δ_k fell below 5.0×10^{-2} we detected convergence of the manifold to a stable periodic solution.

4 The Bifurcation Diagram

The general picture of the dynamics of the PCF laser is that, as $\kappa\tau$ is changed, the laser produces stable periodic output interspersed with 'bubbles' of more complicated dynamics, which for the most part are chaotic [15,16]. We consider in detail a transition to chaos at the beginning of the 'second bubble', in the range of $\kappa\tau \in [2.300, 2.800]$. This transition is outlined in Figure 2, which shows two bifurcation diagrams, one obtained by simulation [Fig. 2(a)] and one by continuation [Fig. 2(b)].

4.1 Simulation

To obtain Figure 2(a), for each value of $\kappa\tau$ we integrated system (1) starting with an initial condition from the attractor for the previous value of $\kappa\tau$ and let transients die away. Then we plotted the normalised value of the inversion $\hat{N} = (N/N_{sol} - 1) \times 10^3$ whenever the intensity $P = |E|^2$ crossed its average value in the increasing direction. This section was chosen to ensure intersections of the orbit for distinct values of the inversion N [16]. In Fig. 2(a), a small number of points correspond to a periodic solution. A large number of points correspond to quasiperiodic or chaotic dynamics.

Figure 3 shows the associated representative phase portraits, obtained by simulation, of the dynamics corresponding to Figure 2(a), shown in projection onto (E, N)-space (top) and the E-plane (middle). We also show associated intersections of the orbits with a plane Σ (bottom). Throughout this paper, we fix the plane

$$\Sigma \equiv \{ (E, N) \mid N = 7.620 \times 10^8 \}.$$

The value $N = 7.620 \times 10^8$ was chosen because it is a good approximation to the average value of N for all $\kappa\tau$ in our region of interest, ensuring that all attractors intersect Σ over the entire range of $\kappa\tau$ considered. We remark that the exact choice of Σ is not important, as long as orbits intersect transversally at least locally near the relevant periodic orbits.

Figures 2(a) and 3 indicate the following bifurcation scenario of symmetric attractors. The periodic solution at $\kappa\tau = 2.300$ is destabilised in a torus bifurcation T at $\kappa\tau \approx 2.307$. The ensuing dynamics is quasiperiodic and takes place on an attracting torus, shown in Figure 3(b). At $\kappa\tau \approx 2.441$ the dynamics on the torus becomes locked to a stable periodic solution in a saddle-node bifurcation of limit cycles SL. This stable orbit can be seen in Figure 3(c) as a period-five solution, and it is responsible for the five branches in Figure 2(a). This stable solution itself undergoes a torus bifurcation T at $\kappa\tau \approx 2.556$, re-

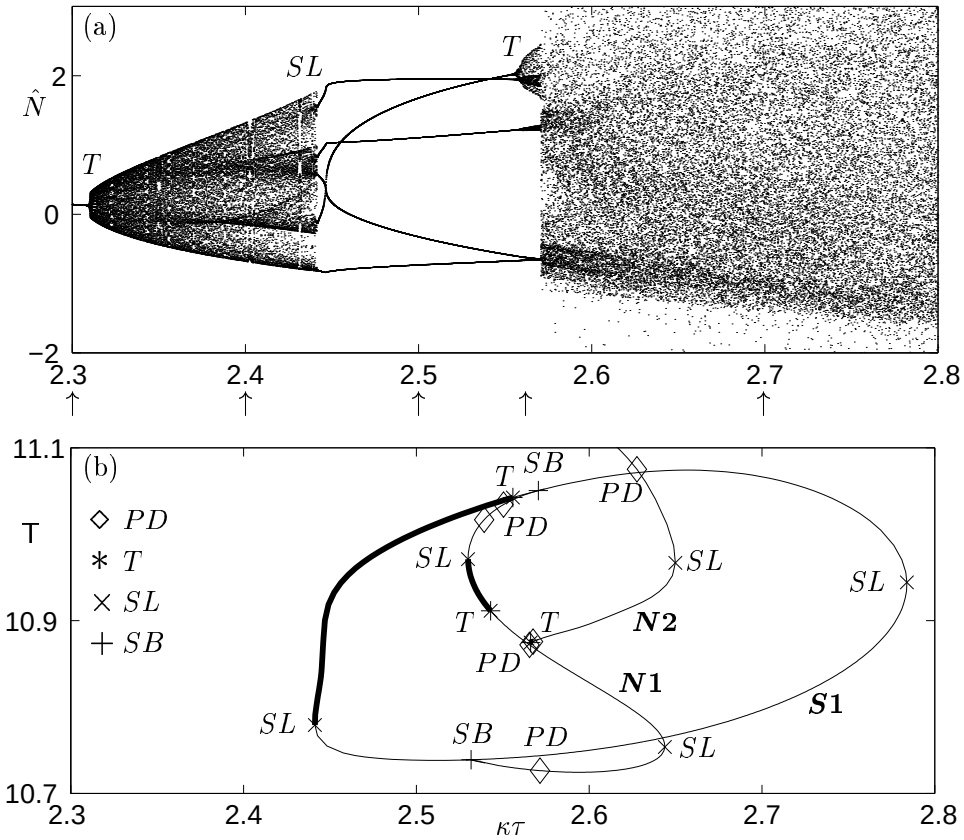

Fig. 2. Bifurcation diagram obtained by simulation (a), and by continuation with DDE-BIFTOOL (b). The consecutive arrows correspond to the phase portraits shown in Fig. 3(a)–(e).

sulting in quasiperiodic modulations of the laser output. The associated new torus is essentially a 'hose-like' object wrapped around the remainder of the initial torus; see Figure 3(d) where we see the torus as a thicker version of the period-five locked solution [Fig. 3(c)]. It is further confirmed by close inspection of the attractor in Σ that there are indeed invariant circles located around the previously locked solution. This new torus is destroyed at $\kappa\tau \approx 2.570$ and the dynamics becomes chaotic. By comparing simulations for increasing and decreasing $\kappa\tau$, we found that there is no hysteresis in this transition.

A similar route to chaos has been observed, by simulation, in a semiconductor laser with COF [8]. However, no explanation was given as to why there was a sudden transition to a large chaotic attractor. Therefore, an immediate question is: What is the mechanism involved in the sudden transition from the attracting torus to a much larger chaotic attractor? We answer this question in Section 6, where we identify this transition to chaos as a crisis bifurcation. This requires the new technique of computing 1D unstable manifolds of system (1).

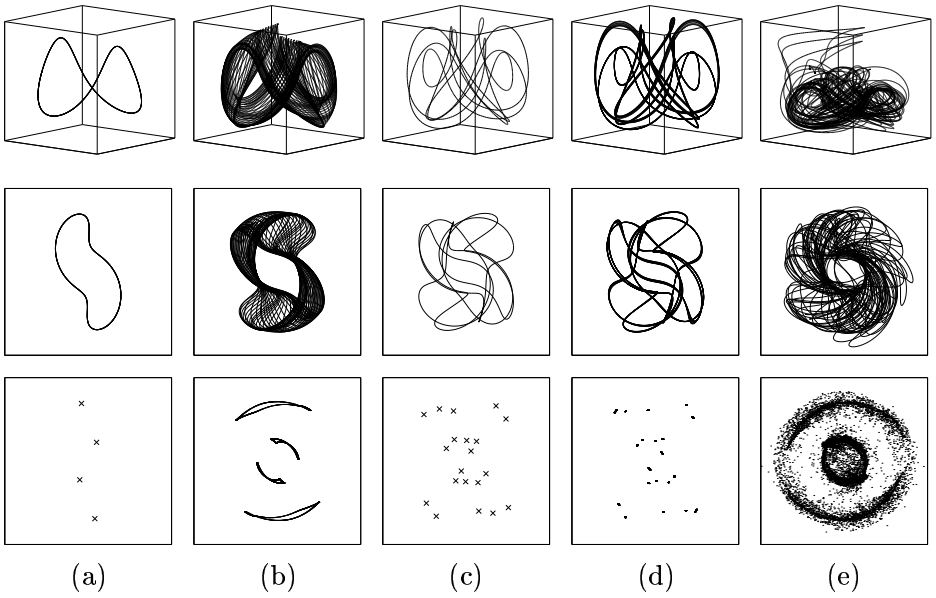

Fig. 3. Phase portraits shown in projection onto (E, N)-space (top) and onto the E-plane (middle); along with associated intersections with the plane $\Sigma \equiv \{N = 7.620 \times 10^8\}$ shown in projection onto the E-plane (bottom). From (a) to (e) $\kappa\tau$ takes the values 2.300, 2.400, 2.500, 2.562, and 2.700.

4.2 Continuation

Figure 2(b) was obtained with DDE-BIFTOOL by starting a continuation from the stable locked periodic solution on the torus. Plotted is the period T, or $\mathsf{T}/2$ for period-doubled solutions, against $\kappa\tau$. We choose to plot T as is often done in continuation studies to ensure a smooth solution branch as $\kappa\tau$ is varied. Attracting solutions are drawn as thick curves, while unstable solutions are thin. By studying the Floquet multipliers of the system we are able to identify the bifurcations involved, namely, saddle-node bifurcations of limit cycles SL, period-doubling bifurcations PD and torus bifurcations T. Due to the underlying symmetry of system (1) we also find symmetry-breaking bifurcations SB of a symmetric periodic orbit. Here a real Floquet multiplier passes through the unit circle at $+1$. As opposed to a saddle-node bifurcation of limit cycles, this leads to the creation of two non-symmetric periodic orbits. Symmetry-breaking bifurcations can be distinguished from saddle-node bifurcations of limit cycles by looking at where they appear on branches. Using the new functionality of DDE-BIFTOOL described in Section 3, we switched onto and computed the emanating branches of non-symmetric periodic solutions. Figure 2(b) shows an oval branch $\boldsymbol{S1}$ of symmetric periodic solutions and two branches $\boldsymbol{N1}$ and $\boldsymbol{N2}$ of non-symmetric periodic solutions. We will refer to $\boldsymbol{S1}$ as having a lower and an upper part, bounded by the saddle-node bifurcations of limit cycles SL at the maximum and minimum values of $\kappa\tau$.

The main stable solution, indicated by a thick line, lies on the upper part of $\boldsymbol{S1}$. Analysis of the Floquet multipliers shows that this stable solution is born at SL at $\kappa\tau \approx 2.441$, marking the onset of locking. It destabilises at $\kappa\tau \approx 2.556$ in the torus bifurcation T. This agrees with the simulation in Figure 2(a). The ensuing unstable solution exists until $\kappa\tau \approx 2.784$, where it 'collides' with the lower part of $\boldsymbol{S1}$ and both solutions are lost at SL. Two additional bifurcations of unstable solutions also exist on $\boldsymbol{S1}$. They are symmetry-breaking bifurcations at the points denoted by SB, which are in fact connected by a branch of non-symmetric solutions $\boldsymbol{N1}$.

By continuing the branch $\boldsymbol{N1}$ emanating from the point SB on the lower part of $\boldsymbol{S1}$ at $\kappa\tau \approx 2.532$, we detect a period-doubling bifurcation PD. This leads to a period-doubled bifurcating branch $\boldsymbol{N3}$ (not shown in Figure 2(b); see Figure 10). We then detect a saddle-node bifurcation of limit cycles SL, before a second period-doubling bifurcation PD leading to the branch $\boldsymbol{N2}$. At $\kappa\tau \approx 2.543$ a torus bifurcation T leads to a stable solution on branch $\boldsymbol{N1}$, indicated by the thick curve. This stable solution is destabilised at a saddle-node bifurcation of limit cycles SL at $\kappa\tau \approx 2.530$. The unstable branch then passes two period-doubling bifurcations PD. These are in fact connected via a branch of period-doubled unstable solutions (not shown). Finally, symmetry is restored in the symmetry-breaking bifurcation SB on the upper part of $\boldsymbol{S1}$.

Continuing the period-doubled branch $\boldsymbol{N2}$, we follow an unstable solution and rapidly detect a torus bifurcation T at $\kappa\tau \approx 2.5661$, this leads to another stable solution. This stable solution is almost immediately destabilised in a period-doubling bifurcation PD at $\kappa\tau \approx 2.5675$. This small region of stability is invisible on the scale of Figure 2(b), but it is enlarged in Section 5 below. Through further continuation of branch $\boldsymbol{N2}$, we detected a saddle-node bifurcation and a period-doubling bifurcation before the branch leaves the window of Figure 2(b).

By following bifurcating branches of unstable solutions, we have found values of $\kappa\tau$ for which there exist regions of bistability and multiple unstable solutions. Figure 4 shows an example of such solutions obtained by taking a vertical slice of Figure 2(b), through the central non-symmetric branch $\boldsymbol{N1}$, where we observe different stable and unstable solutions for $\kappa\tau = 2.542$; see also Figure 5(a) below. Plotted are two symmetric orbits on branch $\boldsymbol{S1}$, one stable and one unstable, as well as three non-symmetric orbits on branch $\boldsymbol{N1}$, one stable and two unstable. If symmetric counterparts of the non-symmetric orbits are included, there are eight coexisting periodic solutions, three of which are attractors and five of which are of saddle-type.

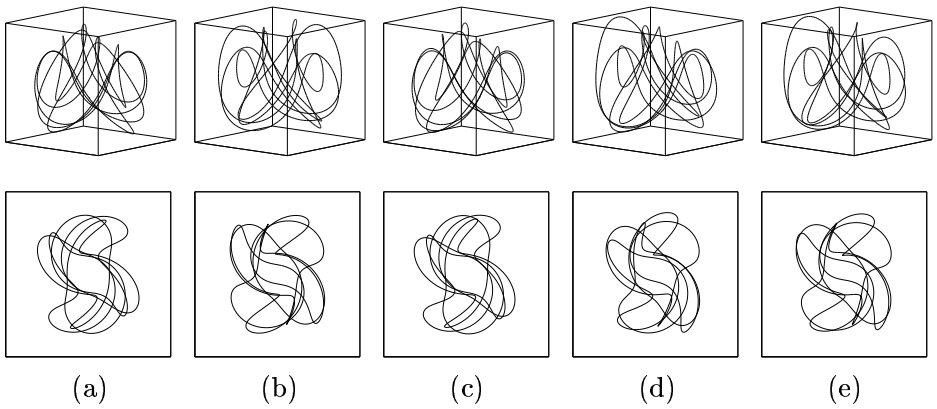

Fig. 4. Periodic orbits shown in projection onto (E, N)-space (top) and onto the E-plane (bottom) for $\kappa\tau = 2.542$. Showing, the symmetric unstable orbit on the lower part of $\boldsymbol{S1}$ (a), the symmetric stable orbit on the upper part of $\boldsymbol{S1}$ (b), the non-symmetric unstable orbit on the lower part of $\boldsymbol{N1}$ (c), the non-symmetric stable orbit on the middle part of $\boldsymbol{N1}$ (d), and the non-symmetric unstable orbit on the upper part of $\boldsymbol{N1}$ (e).

5 Windows of Bistability

We now investigate in detail the two regions of bistability that we identified in Figure 2(b). This bistability is between a symmetric pair of periodic solutions on $\boldsymbol{N1}$ and the main periodic solution on $\boldsymbol{S1}$, and between a symmetric pair of periodic solutions on $\boldsymbol{N2}$ and the 'hose-like' torus shown in Fig. 3(d). Both of the symmetric pairs of periodic solutions have small basins of attraction and, therefore, would be extremely difficult to observe in simulations without using initial conditions obtained by continuation. We remark that there is no hysteresis associated with these stable solutions when one follows the main attractor as in Figure 2(a). This is because the windows of stability are connected to $\boldsymbol{S1}$ via unstable branches, so that, scanning back and forth, in the bifurcation diagram, the dynamics is always attracted to the main attractor.

The first region of stability on $\boldsymbol{N1}$ is illustrated in Figures 5(a) and (b). Continuation shows that a stable periodic orbit is born at $\kappa\tau \approx 2.530$ in a saddle-node bifurcation of limit cycles SL. It exists for $\kappa\tau \in [2.530, 2.543]$. By starting from the attracting periodic solution found with DDE-BIFTOOL [Fig. 5(a)], we can compute a bifurcation diagram by simulation to see what happens to this solution as we increase and decrease $\kappa\tau$ in small steps. This results in the bifurcation diagram of Figure 5(b). As found by continuation, at $\kappa\tau \approx 2.543$, the periodic orbit undergoes a torus bifurcation T. The dynamics then locks to a periodic solution. This locked solution seemingly undergoes a period-doubling cascade to a small region of chaos. After this, the solution jumps to the main attractor of system (1), in this case the stable periodic solution on $\boldsymbol{S1}$. Notice that Figure 5(a) contains ten branches due to the

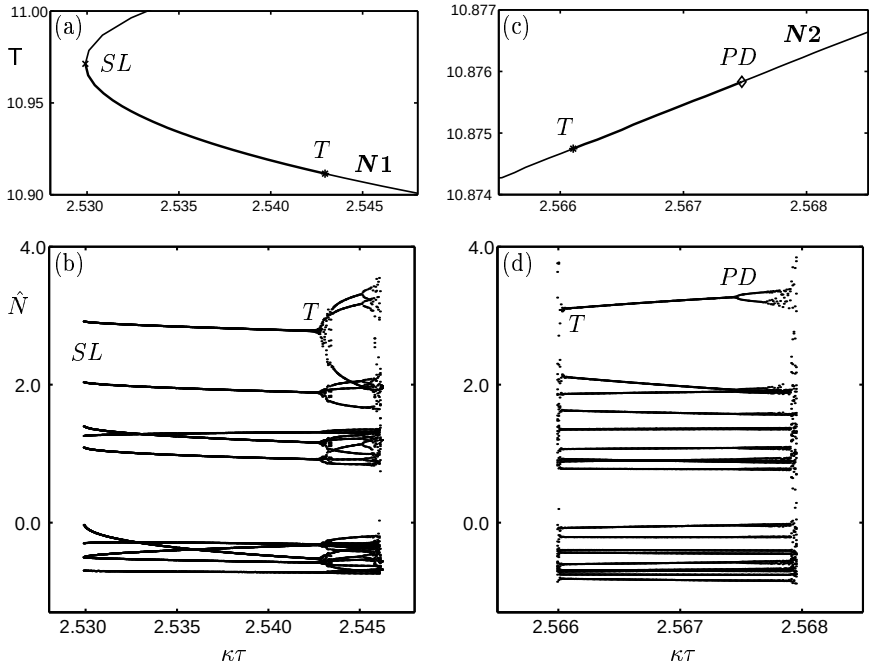

Fig. 5. Bifurcation diagrams near the stable region of branch $\boldsymbol{N1}$, obtained by continuation (a) and by simulation (b), and near the stable region of branch $\boldsymbol{N2}$, again obtained by continuation (c) and by simulation (d).

non-symmetric nature of the solution, the periodic orbit is still of period five.

The region of stability on $\boldsymbol{N2}$ is illustrated in Figures 5(c) and (d). Again, by starting from the attracting periodic solution found with continuation [Fig. 5(c)] and integrating as we increase and decrease $\kappa\tau$ in small steps, we obtain the bifurcation diagram by simulation shown in Figure 5(d). DDE-BIFTOOL detects a stable solution for $\kappa\tau \in [2.5661, 2.5675]$; for this computation the numerical accuracy was increased to ensure a significant fourth decimal place. While this range is below present experimental accuracy, finding this stable region showcases the usefulness of DDE-BIFTOOL. At the left boundary of stability there is a torus bifurcation T. Simulation shows that the emerging torus seemingly breaks up quickly to a small region of chaos. At the right boundary of stability, the stable solution undergoes a period-doubling bifurcation PD. Simulation shows a cascade to a short region of chaos. When leaving the region of stability, the solution jumps to the main attractor of system (1), in this case the attracting 'hose-like' torus. Notice that Figure 5(c) contains twenty branches due to the period-doubled non-symmetric nature of the solution, the periodic orbit is of period ten.

The new attracting periodic solutions, that were found in these simulations, could be continued with DDE-BIFTOOL, but due to the small parameter ranges in which these solutions exist, we stop here. However, the overall picture is again that of the break-up of a torus but on a smaller scale.

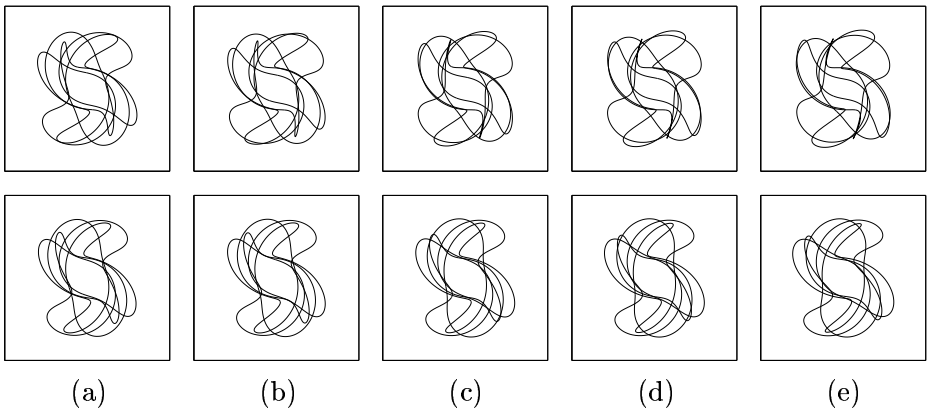

Fig. 6. Symmetric stable orbits (top) and corresponding symmetric unstable orbits (bottom) shown in projection onto the E-plane. From (a) to (e) $\kappa\tau$ takes the values 2.445, 2.450, 2.480, 2.500 and 2.531; the square is $E \in [-400, 400] \times [-400, 400]$.

6 Break-up of a torus

The bifurcation diagrams of Figure 2, along with the phase portraits in Figure 3, present a good picture of the main attractors involved in the break-up of a torus in a semiconductor laser with PCF. However, in order to understand this transition fully, in particular, to understand why we have a sudden change from an attracting torus to a much larger chaotic attractor, we need to investigate what happens to the underlying torus after locking. For this it is not sufficient to use mere simulation, because for $2.440 < \kappa\tau < 2.555$ one will only get an image of the stable periodic orbit [Fig. 3(c)], and not of the torus (or its remainder) on which it lies. This is where our method for the computation of the 1D unstable manifolds of the saddle periodic orbits is crucial.

The saddle periodic orbits we used are along the lower part of $\boldsymbol{S1}$ and are shown in the bottom row of Figure 6. The top row shows the corresponding stable orbits. Both are shown in projection onto the E-plane and the values of parameters are $\kappa\tau = 2.445$, $\kappa\tau = 2.450$, $\kappa\tau = 2.480$, $\kappa\tau = 2.500$ and $\kappa\tau = 2.531$. At these values of $\kappa\tau$, between SL and SB on the lower part of $\boldsymbol{S1}$ [Fig.2(b)], the saddle periodic orbits have exactly one unstable Floquet multiplier and therefore, their unstable manifolds are one dimensional. This allows us to compute them with the methods outlined in Section 3.

In Figure 7 we show the trace of these unstable manifolds in the plane Σ. The crosses (+) mark the five intersection points with Σ of the saddle periodic orbit in Figure 6. From each saddle point there emanate two branches of the unstable manifold, which converge to neighbouring attracting points ($\times$) corresponding to the stable periodic orbit in Figure 6. In this way and much like for ODEs, the torus, or what remains of it is the closure of these

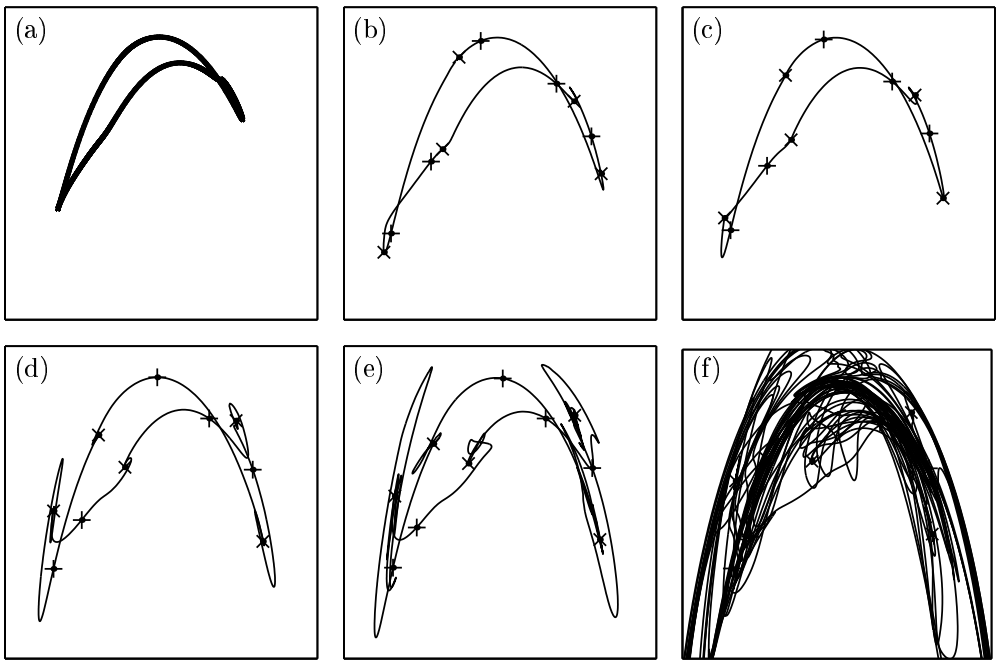

Fig. 7. Break-up of the torus in the plane $\Sigma \equiv \{N = 7.620 \times 10^8\}$. Except for (a), which was obtained by simulation, plotted are all branches of the 1D unstable manifolds of the saddle points (+), which converge to the attractors (×). From (a) to (f) $\kappa\tau$ takes the values 2.400, 2.445, 2.450, 2.480, 2.500 and 2.531; the square is $E \in [-300, 300] \times [140, 300]$.

branches of the 1D unstable manifold, and it shows up as a closed curve. Note that there are twenty intersections associated with locking on the full torus [Fig. 3(c)]. They correspond to the torus intersecting four times resulting in four groups of five intersections. We show only the top five intersections. Recall that the different branches of the unstable manifold are allowed to intersect each other because we are looking at a two-dimensional projection of an infinite-dimensional system.

Our computations reveal the following bifurcation scenario as $\kappa\tau$ is increased through the locking region. The locking of the quasiperiodic solution [Fig. 7(a)] produces a stable periodic solution that exists on a smooth torus [Fig. 7(b)], as one expects immediately after locking. However, smoothness is lost as the manifold starts to 'curl up' along the stable periodic orbit. DDE-BIFTOOL detects this transition at $\kappa\tau \approx 2.4502$, where we found that the two Floquet multipliers close to and inside the unit circle become a complex pair. Figure 7(c) shows the manifold just after this transition at $\kappa\tau = 2.450$. Notice that the branches of the manifold are no longer smoothly connected at the attractors (×) but now spiral into them. Physically, this corresponds to damped oscillations of the laser output as it settles down to its periodic solution. The unstable manifold becomes increasingly folded and stretched as $\kappa\tau$ is increased and the chaotic region is approached. Nevertheless, the torus is

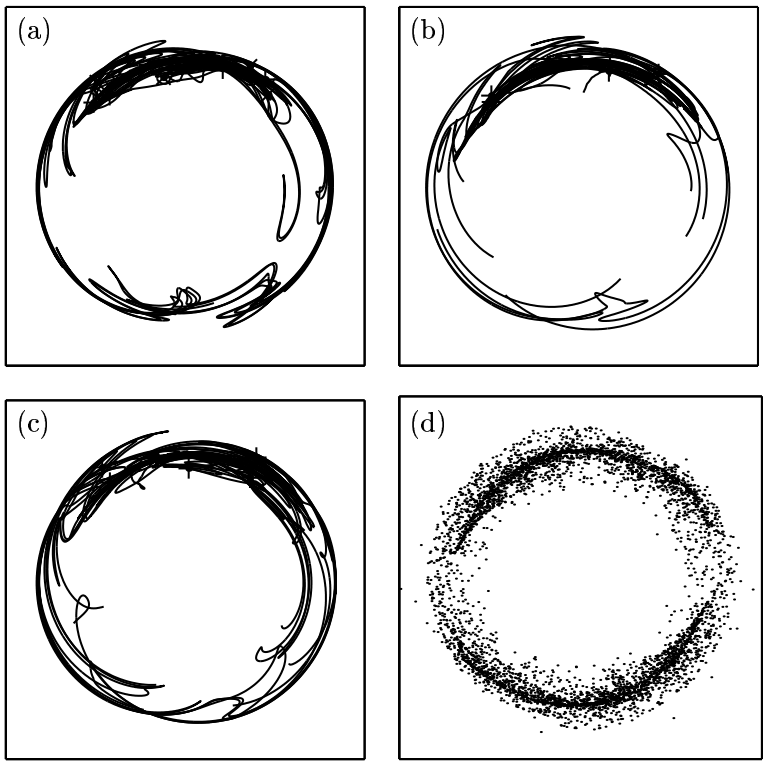

Fig. 8. Break-up of the torus in the plane $\Sigma \equiv \{N = 7.620 \times 10^8\}$. Plotted are all branches of the 1D unstable manifolds for $\kappa\tau = 2.531$ (a) and $\kappa\tau = 2.700$ (b) on the lower part of $\boldsymbol{S1}$, for $\kappa\tau = 2.700$ on the upper part of $\boldsymbol{S1}$ (c) and the associated intersection of the main attractor for $\kappa\tau = 2.700$ (d); the square is $E \in [-400, 400] \times [-400, 400]$.

still a continuous (but not a smooth) object [Figs. 7(d) and (e)]. The transients are becoming increasingly complicated as $\kappa\tau$ is increased. At $\kappa\tau = 2.531$ we see the unstable manifold covering a large part of the upper part of the E-plane [Fig. 7(f)] and also making excursions into the lower part; see already Figure 8(a) which shows the 1D unstable manifold of Figure 7(f) over a larger area of the E-plane. Note that Figure 8 still shows the 1D unstable manifold associated with only the top group of five of the twenty intersections of the saddle periodic orbit with Σ.

At $\kappa\tau \approx 2.5348$ the saddle periodic orbit undergoes a symmetry-breaking bifurcation SB, resulting in an additional unstable direction of the unstable manifold. However, it is still possible to compute the *strong unstable manifold*, corresponding to the largest, real Floquet multiplier of the associated periodic orbit [23]. This strong unstable manifold is shown in Figure 8 inside the chaotic region for the saddle periodic orbit on the lower part of $\boldsymbol{S1}$ at $\kappa\tau = 2.700$ [Fig. 8(b)]. It is indeed a continuation of the unstable manifold for $\kappa\tau = 2.531$ [Fig. 8(a)].

We also computed 1D unstable manifolds for the saddle periodic orbits along

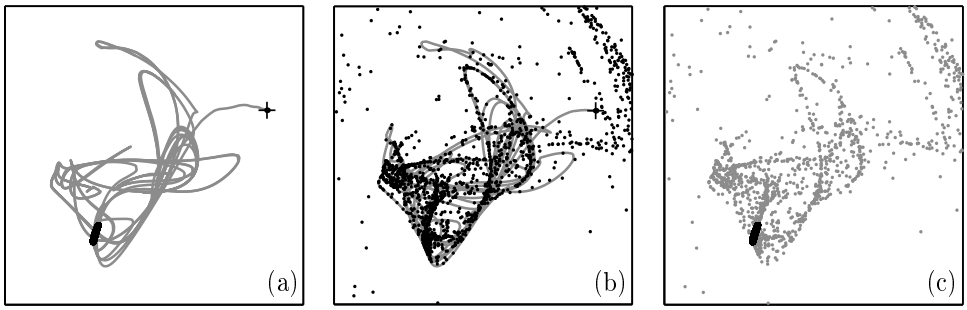

Fig. 9. Crisis bifurcation of the hose-like torus leading to a much larger chaotic attractor. Plotted is one branch of the 1D unstable manifold (grey curve) and the associated main attractor (black dots) before the crisis for $\kappa\tau = 2.569$ (a) and after the crisis for $\kappa\tau = 2.571$ (b). Panel (c) is an overlay of the hose-like torus (black) and the chaotic attractor (grey) that exist before and after the crisis bifurcation, respectively; the square is $E \in [-95, 105] \times [235, 275]$.

the upper part of $\boldsymbol{S1}$ between SB and SL. Here the saddle orbits have exactly one unstable Floquet multiplier and, therefore, also have one unstable direction. An associated unstable manifold, for $\kappa\tau = 2.700$, is shown in Figure 8(c). We observe that it is very similar to the unstable manifold in Figure 8(b). As is generally the case, the unstable manifold accumulates on the chaotic attractor. To illustrate this, the associated intersection with Σ of the upper and lower parts of the main chaotic attractor for $\kappa\tau = 2.700$ is shown in Figure 8(d).

The sudden transition to chaos at $\kappa\tau \approx 2.570$ is indicative of a crisis bifurcation, in which we see a discontinuous change in the size or shape of an attractor [37–39]. In our case this attractor is the hose-like torus. At the crisis bifurcation there is a rearrangement of stable and unstable manifolds of suitable saddle points. It is not possible to compute the infinite-dimensional stable manifold of a saddle point in a DDE. However, we can cast more light on this bifurcation by computing the branch of the 1D unstable manifold that ends up at the attractor. This is shown in Figure 9 (a) and (b) for one (of the five) saddle points corresponding to the saddle periodic orbit; compare Figure 2 (b). Just before the crisis bifurcation at $\kappa\tau = 2.569$ [Fig. 9 (a)] the unstable manifold is contained in the basin of attraction of the hose-like torus and, hence, eventually ends up at the corresponding attracting invariant circle. Notice however, that this branch makes large excursions before settling down. After the crisis bifurcation at $\kappa\tau = 2.571$ [Fig. 9 (b)] the hose-like torus has seemingly been replaced by a much larger chaotic attractor. The unstable manifold accumulates on this new attractor, which has a shape resembling the manifold just prior to the bifurcation. However, the chaotic attractor is no longer confined by the stable manifold of the saddle. Overlaying the attractor before and after the crisis bifurcation [Fig. 9 (c)] shows that the hose-like torus is 'part of' the large chaotic attractor. In other words, in the crisis bifurcation

a small 'regular' attractor (an invariant torus) suddenly and discontinuously changes in size to become a chaotic attractor.

The crisis bifurcation we found in the PCF laser is much like an interior crisis in that there is a sudden growth in the size of the attractor. However, the smaller attractor is not chaotic itself (as is generally assumed in the definition of an interior crisis [37–39]). We remark that the sudden appearance of the much larger chaotic attractor is preceded by more and more complex transients due to the increasingly complicated geometry of unstable manifolds; see Figs. 7–9.

7 Conclusions and Discussion

In summary, we have presented a detailed numerical investigation of a route to chaos via the break-up of a torus in a PCF laser. A similar transition has also been observed in a COF laser [8] but the actual sudden transition to the chaotic attractor has not been explained. Our results clearly indicate that the chaotic attractor associated with this transition was created at a crisis bifurcation. We believe this to be the first time that a sudden transition to chaos has been studied in detail in a system of DDEs. This was only made possible by advanced numerical tools for DDEs, namely the package DDE-BIFTOOL to compute saddle periodic orbits, combined with our new technique for computing unstable manifolds of saddle periodic orbits. This highlights the use of these techniques for DDEs in general.

As an indication of the overall complexity of the bifurcation diagrams, Figure 10 shows the further continuation of branch $\boldsymbol{N2}$ and the continuation of another branch of non-symmetric solutions $\boldsymbol{N3}$ from a period-doubling bifurcation of branch $\boldsymbol{N1}$. Branches $\boldsymbol{N2}$ and $\boldsymbol{N3}$ both end in period-halving bifurcations, at $\kappa\tau \approx 2.6063$ and $\kappa\tau \approx 2.5893$ respectively, leading to another branch of non-symmetric solutions $\boldsymbol{N4}$. Here we clearly see multiple solutions existing for small intervals of $\kappa\tau$. Branches $\boldsymbol{N2}$ and $\boldsymbol{N3}$ contain a number of saddle-node bifurcations of limit cycles SL and period-doubling bifurcations PD, the latter lead to other branches which could be continued. Moreover, at the end of branch $\boldsymbol{N3}$ we find a small region of stability which undergoes a period-halving bifurcation leading to a small region of stability on branch $\boldsymbol{N4}$ for $\kappa\tau \in [2.5832, 2.5893]$. We found that these stable solutions have such small basins of attraction that it is numerically very difficult to find the stable solution even when starting from the numerical approximation provided by DDE-BIFTOOL. We believe that the period-doubling of this stable solution on branch $\boldsymbol{N4}$ is the start of a period-doubling cascade to chaos. If this is the case, it implies the coexistence of two chaotic attractors.

We note here that the symmetry-breaking bifurcation SB on the upper part of

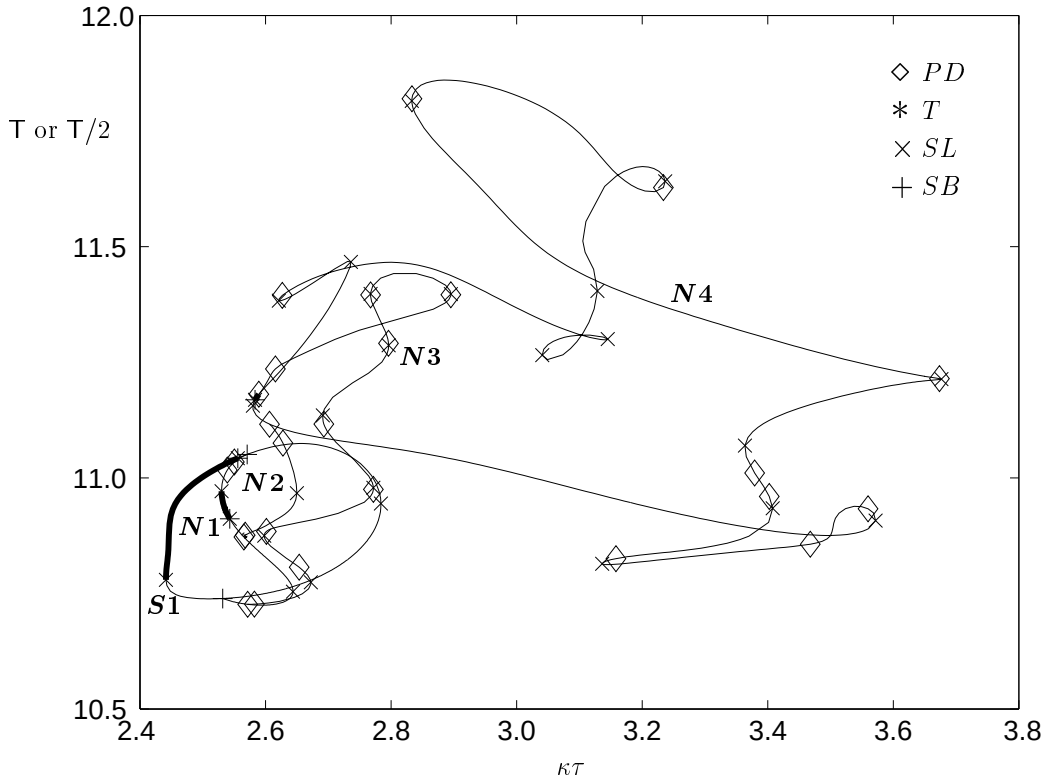

Fig. 10. Bifurcation diagram obtained by continuation showing the branches $\boldsymbol{N2}$ and $\boldsymbol{N3}$, which are connected to a further bifurcating branch $\boldsymbol{N4}$.

$\boldsymbol{S1}$ [Fig. 2(b)] appears to coincide with the value of $\kappa\tau$ at which we identified the crisis bifurcation. A possible explanation connecting these two events is as follows. As SB is approached along branch $\boldsymbol{N1}$, the non-symmetric orbit tends to the symmetric orbit of branch $\boldsymbol{S1}$. The fact that these two periodic orbits come together implies that a much larger phase space can be visited by the unstable manifold. Eventually at SB the periodic orbits coincide and we see the sudden emergence of the chaotic attractor.

We conclude with some questions for future work. What happens if we continue the periodic solutions found between the bubbles of chaos? These solutions correspond to the power oscillating at the frequency of the *external-cavity modes* (ECMs) of the PCF laser, which oscillate at approximately an integer multiple of the fundamental external-cavity frequency $1/\tau$. The periodic solution of Figure 2(a), shown for $\kappa\tau \in [2.300, 2.307]$, is the first of these ECM solutions. Investigations indicate that all ECM solutions between the bubbles of chaos at higher values of $\kappa\tau$ are connected via branches of unstable solutions to an (unstable) equilibrium existing close to locking for small values of $\kappa\tau$. For a detailed study of the ECMs of the PCF laser we refer to Ref. [33].

There is a lot of current interest in the dimensionality of attractors in lasers with delay, particularly for use in communication schemes [40]. We remark

that the transition outlined in this paper, up to and including the chaotic region, can occur in a phase-space of minimal dimension three. What are the mechanisms involved in the routes to chaos for higher values of $\kappa\tau$? Are these transitions to 'high dimensional chaos'? We believe that the techniques described in this paper will contribute to answering these questions.

Acknowledgements

The authors thank Sebastian Wieczorek for helpful discussions. B. K. is supported by an EPSRC Advanced Research Fellowship. The work of K. E. was partially funded by the Research Project OT 98/16, funded by the Research Council K. U. Leuven and of the Research Project G.0270.00 funded by the Fund for Scientific Research - Flanders (Belgium).

References

[1] G. H. M. van Tartwijk and G. P. Agrawal. Laser instabilities: a modern perspective. Progr. Quantum Electron., **22**, 43 (1998).

[2] B. Krauskopf and D. Lenstra, editors. Fundamental Issues of Nonlinear Laser Dynamics, AIP Conference Proceedings, **548** (2000).

[3] R. D. Driver. Ordinary and Delay Differential Equations, (Springer-Verlag, Berlin, 1977).

[4] J. K. Hale, S. M. Verduyn Lunel Introduction to Functional Differential Equations, (Springer-Verlag, 1993).

[5] O. Diekmann, S. A. van Gils, S. M. Verduyn Lunel, H. -O. Walther. Delay Equations: Functional-, Complex-, and Nonlinear Analysis, (Springer-Verlag, 1995).

[6] S. M. Verduyn Lunel and B. Krauskopf. The mathematics of delay equations with an application to the Lang-Kobayashi equations. In [2], pp 66–86.

[7] A. Gavrielides. Nonlinear Dynamics of Semiconductor Lasers: Theory and Experiments. In [2], pp 191–217.

[8] J. Mørk, B. Tromborg and J. Mark. Chaos in Semiconductor Lasers with Optical Feedback: Theory and Experiment. IEEE J. Quantum Elec., **28**, 93 (1992).

[9] T. Heil, I. Fischer, W. Elsässer. J. Mulet and C. R. Mirasso. Chaos Synchronization and Spontaneous Symmetry-Breaking in Symmetrically Delay-Coupled Semiconductor Lasers. Phys. Rev. Lett., **86**, 795 (2001).

[10] X. S. Yao and L. Maleki. Dual Microwave and Optical Oscillator. Opt. Letters, **22**, 1867 (1997).

[11] C. R. Giuliano. Applications of optical phase conjugation. Physics Today, pp 27–35, April 1981.

[12] G. R. Gray, D. H. DeTienne and G. P. Agrawal. Mode locking in semiconductor lasers by phase-conjugate optical feedback. Opt. Lett., **20**, 1295 (1995).

[13] G. P. Agrawal and G. R. Gray. Effect of phase-conjugate feedback on the noise characteristics of semiconductor lasers. Phys. Rev. A, **46**, 5890 (1992).

[14] G. H. M. van Tartwijk, H. J. C. van der Linden and D. Lenstra. Theory of a diode laser with phase-conjugate feedback. Opt. Lett., **17**, 1590 (1995).

[15] G. R. Gray, D. Huang, and G. P. Agrawal. Chaotic dynamics of semiconductor lasers with phase-conjugate feedback. Phys. Rev. A, **49**, 2096 (1994).

[16] B. Krauskopf, G. R. Gray, and D. Lenstra. Semiconductor laser with phase-conjugate feedback: Dynamics and bifurcations. Phys. Rev. E, **58**, 7190 (1998).

[17] G. D. Van Wiggeren and R. Roy. Communication with Chaotic Lasers. Science, **279**, 1198 (1998).

[18] I. Fischer, Y. Liu and P. Davis. Synchronization of chaotic semiconductor laser dynamics on subnanosecond time scales and its potential for chaos communication. Phys. Rev. A, **62**, 011801 (2000).

[19] K. Engelborghs, T. Luzyanina, K. in't Hout and D. Roose. SIAM J. Sci. Comput. **22**, 1593 (2000)

[20] K. Engelborghs, T. Luzyanina and D. Roose. J. Comput. Appl. Math. **125**, 265 (2000)

[21] K. Engelborghs. 'DDE-BIFTOOL: a Matlab package for bifurcation analysis of delay differential equations'. `http://www.cs.kuleuven.ac.be/~koen/delay/ddebiftool.shtml`

[22] E. Doedel, T. Fairgrieve, B. Sandstede, A. Champneys, Yu. Kuznetsov and X. Wang. 'AUTO 97: Continuation and bifurcation software for ordinary differential equations'. `http://indy.cs.concordia.ca/auto/main.html`

[23] B. Krauskopf and K. Green. Computing unstable manifolds in delay differential equations, J. Comput. Phys., to appear.

[24] J. D. Murray. Mathematical Biology, Biomathematics Texts, **19**, (Springer-Verlag, Berlin, 1980).

[25] C. M. Marcus and R. M. Westervelt. Stability of analog networks with delay. Phys. Rev. A, **39**, 347 (1989).

[26] H. Glüsing-Lüerssen. A behavioral approach to delay-differential systems. SIAM J. Control Optim., **35**, 480 (1997).

[27] D. Pieroux, T. Erneux, T. Luzyanina and K. Engelborghs. Interacting pairs of periodic solutions lead to tori in lasers subject to delayed feedback. Phys. Rev. E, **63**, 036211 (2001).

[28] D. Pieroux, T. Erneux, B. Haegeman, K. Engelborghs and D. Roose. Bridges of periodic solutions and tori in semiconductor lasers subject to delay. Phys. Rev. Lett., **87**, 193901 (2001).

[29] T. W. Carr, D. Pieroux and P. Mandel. Theory of a multimode semiconductor laser with optical feedback. Phys. Rev. A, **63**, 033817 (2001).

[30] B. Haegeman, K. Engelborghs, D. Roose, D. Pieroux and T. Erneux. Rupture of bifurcation bridges in semiconductor lasers subject to optical feedback. Phys. Rev. E, to appear.

[31] M. Sciamanna, T. Erneux, F. Rogister, O. Deparis, P. Mégret and M. Blondel. Bifurcation bridges between external-cavity modes lead to polarization self-modulation in vertical-cavity surface emitting lasers. Phys. Rev. A, **65**, 041801(R) (2002).

[32] K. Green and B. Krauskopf. Global bifurcations and bistability at the locking boundaries of a semiconductor laser with phase-conjugate feedback. Phys. Rev. E, 073207 (2002).

[33] K. Green and B. Krauskopf. Bifurcation analysis of frequency locking in a semiconductor laser with phase-conjugate feedback. Int. J. Bifurcation and Chaos, to appear.

[34] B. Krauskopf, G. H. M. van Tartwijk, and G. R. Gray. Symmetry properties of lasers subject to optical feedback. Opt. Commun., **177**, 347 (2000).

[35] Y. Kuznetsov. Elements of Applied Bifurcation Theory (Springer, Berlin, 1995).

[36] B. Krauskopf and H. Osinga. Growing 1D and Quasi-2D Unstable Manifolds of Maps. J. Comput. Phys., **146**, 404 (1998).

[37] C. Grebogi, E. Ott and J. A. Yorke. Critical Exponent of Chaotic Transients in Nonlinear Dynamical Systems. Phys. Rev. Lett., **57**, 11 (1986)

[38] C. Grebogi, E. Ott, F. Romeiras and J. A. Yorke. Critical exponents for crisis-induced intermittency. Phys. Rev. A, **36**, 11 (1987)

[39] C. Robert, K. T. Alligood, E. Ott and J. A. Yorke. Explosions of chaotic sets. Physica D, **144**, 44 (2000).

[40] J. K. White and J. V. Moloney. Multichannel communication using an infinite dimensional spatiotemporal chaotic signal. Phys. Rev. A, **59**, 2422 (1999).